Multiporous Polymeric Materials from Thermoreversible Poly(vinylidene fluoride) Gels

Debarshi Dasgupta and Arun K. Nandi*

Polymer Science Unit, Indian Association For the Cultivation of Science, Jadavpur, Kolkata 700032, India

Received March 22, 2005; Revised Manuscript Received May 28, 2005

ABSTRACT: Thermoreversible gels of poly(vinylidene fluoride) (PVF_2) in organic diesters [$(CH_2)_n-(COOEt)_2$] were dried by replacing the high boiling diesters with a guest solvent cyclohexane and followed by leaching with methanol. The porosity of the samples was measured using mercury intrusion porosimetry (MIP) for pore size > 6 nm and by nitrogen adsorption porosimetry using the Barett−Joyner−Halenda (BJH) technique for pore size 3−6 nm. Samples dried from gels in diethyl adipate ($n = 4$), diethyl suberate ($n = 6$), and diethyl azelate ($n = 7$) were studied. Porosity in different dimensions, e.g., micro, meso, and macro sizes, was observed in the same sample making them as multiporous materials. Both nano- and macroporosity increase with increasing "*n*" of diesters, and pore volumes and surface areas were also found to increase in a similar fashion. Field emission scanning electron micrographs also support the above points. The differential scanning calorimeteric thermograms at higher heating rate (40 °C/min) show two peaks; the higher melting peak increases with decreasing "*n*". The porous PVF_2 materials have α-polymorphic structure as evidenced from X-ray diffraction. Both nano- and macroporosity decrease with increasing polymer concentration in the gel. The materials show hysteresis loop in the intrusion and extrusion histograms of MIP and nitrogen adsorption porosimetry, indicating ink bottle or interconnected channel structure in the material. Samples dried from increased polymer concentration in the gel have lower nanopore concentration, lower surface area, and lower pore volume.

Introduction

For the past two decades, porous materials are a vibrant area of research because of their potential applications in sorption, catalysis, dielectric materials, and separation processes.[1−7] They are usually classified as microporous, mesoporous, and macroporous depending on their pore sizes. Microporous materials have pore diameters 0.5−2 nm, mesoporous materials have pore diameters 2−50 nm, and macroporous materials have pore diameters >50 nm.[1,8] A combination of micro- and mesoporosity is called as nanoporosity and a combination of micro-, meso-, and macroporosity in the same material is collectively referred to here as multiporous material. Using the supramolecular organization technique, some workers produced organic porous materials;[9,10] however, in such cases the porosity is limited to a particular value of micro- or mesoporosity. Techniques to produce porous polymer materials are temperature-induced phase separation,[11,12] foaming,[13,14] phase inversion,[3,4] etc.; each has advantages in their own area of applications defined by pore size and shape, surface area, pore volume, and material properties. But in these methods the pores are macropores, and also the pore size distribution is not large. It may be needed multiporous material for the separation processes; for example, the recycling of municipal and industrial wastewater is now necessary as supply of freshwater gradually decreases. To separate various sized dissolved organic impurities (like pesticides, insecticides, herbicides, and low molecular weight organics) and inorganic impurities (like arsenic, lead, mercury, and iron salts) from the wastewater, multiporous materials may be necessary. It may be mentioned here that emptied calthrate of syndiotactic polystyrene absorbs dissolved dichlorobenzene (0.5% w/v) in water by half an hour.[15] Recently, Guenet et al. proposed that multiporousity of nanometer and subnanometer dimensions might be achieved by drying thermoreversible polymer gels.[16] In this paper we shall delineate a process of developing multiporous materials from thermoreversible polymer gels where the network junctions arise from physical cross-linking.[17−19]

Poly(vinylidene fluoride) (PVF_2) is a technologically important polymer[20] and is highly used as membrane (Millipore) for its excellent processability, chemical resistance, and good thermal properties.[21] Recent developments in the modification of membrane properties by making graft copolymer with poly(acrylic acid) (PAA) and poly(oxyethylene methacrylate) (POEM) yielded membranes with PH sensitivity and antifouling properties, respectively.[2−4,7] The commercial PVF_2 membranes have mean pore diameter 570, 1410, and 1960 nm, and on grafting with acrylic acid (AAc) average pore sizes of the films were found to be 1660 and 1520 nm for the grafting level ($[AAc]/[PVF_2]_{surface}$) 1.2 and 2.46, respectively.[3] So the average pore size of these films indicates that they are macroporous. It is the aim of this work how micro- and mesoporosity can be introduced in these PVF_2 membranes suitable for the separation of different sized (nano to macro) impurities and also of different chemical nature.

Poly(vinylidene fluoride) produces thermoreversible gels in organic diesters [$(CH_2)_n-(COOEt)_2$].[22,23] The fibrillar network structure is produced due to polymer solvent complexation and with increasing number of carbon atoms in diesters the fibrils become finer. The PVF_2−diethyl azelate (DEAZ, $n = 7$) gel has the finest fibrillar morphology and has been attributed for the formation of the most stable polymer solvent complexes in the series due to the increased enthalpic and entropic effect.[23] Further from the phase diagram it was concluded that the polymer solvent complexes produced are

* To whom correspondence should be addressed: e-mail psuakn@mahendra.iacs.res.in.

10.1021/ma050601g CCC: $30.25
Published on Web 06/24/2005

Scheme 1. An Approximate Molecular Model of PVF_2–DEAZ Gel Obtained from Energy Minimization through MMX Program[a]

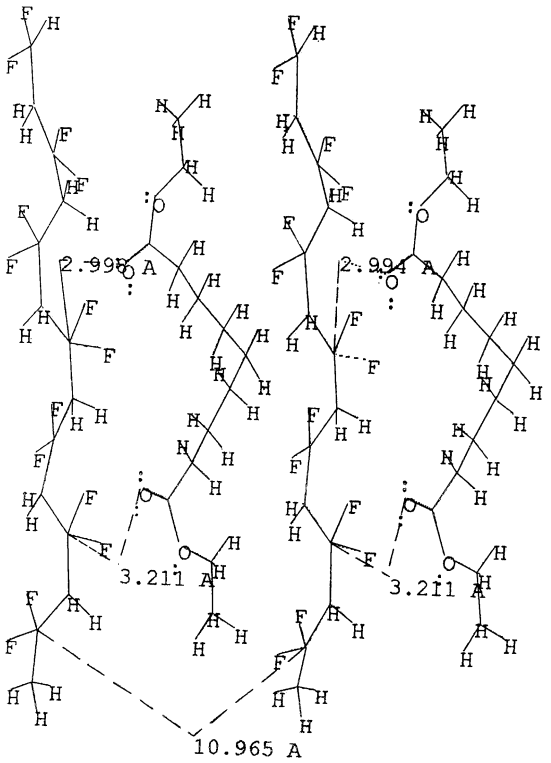

[a] Distances shown are queried from energy-minimized structure.

incongruent or singular type emphasizing that the solvent molecules can be easily removed without disrupting the polymer structure.[22,23] An approximate molecular model of PVF_2–DEAZ gel obtained from energy minimization through a molecular mechanics (MMX) program[24] is shown in Scheme 1. The distances queried (e.g., 2.99, 3.21, 2.99, and 3.21 Å) between ⟩C═O and ⟩CF_2 groups are much lower than the summation of van der Waals radii of the above two groups (e.g., 3.65 Å),[23] supporting the possibility of polymer–solvent complex formation. An important consequence of this model is that the distances between the two PVF_2 chains is about 11 Å, and if the solvent molecules are removed without disturbing the polymer structure, channel type pores of diameter 1.1 nm should be obtained. Further, these thermoreversible gels obey a three-dimensional percolation model[22,25–28] though recently some controversy arises for the applicability of percolation model in these gels.[29] So drying of these gels by keeping the polymer structure intact would produce pores of different diameter from nano to macro dimension, the former would originate from polymer–solvent complexation and the latter from the caging of solvent molecules by the fibrils. Thus, there is a possibility to obtain multiporous materials after proper drying.

Drying of these high boiling diesters from the gels is a difficult problem as heat treatment melts the gel (cf. phase diagram of refs 22 and 23). So an attempt has been made to replace the diester molecules in the calthrate by lower boiling solvent (guest) molecules. These guest solvents usually keep the calthrate structure intact even after drying as reported in syndiotactic polystyrene (s-PS) gels.[30] Here we have chosen cyclohexane with an approximate diameter of 5 Å (calculated using the MMX program[24]) such that the size is lower than that between the polymer strands in the gel. Also, there is no functional group capable of specific interaction with the polymer strand, so there is no chance of any change in the polymer structure by the guest molecules. The boiling point of cyclohexane (80 °C) is much lower than that of diesters (bp of diethyl adipate (DEA) = 251 °C, DES = 282 °C, and DEAZ = 170 °C (18 mmHg)). Finally, cyclohexane is miscible with the diester so it would gradually replace the DEAZ molecules. After removal of diesters by cyclohexane from the gel, it was dried to obtain the porous material.

In this paper we report the porosity of the above materials measured from mercury intrusion porosimetry (MIP) and also from N_2 adsorption porosimetry using Barett–Joyner–Halenda (BJH) method. Both measurement techniques are needed as the MIP limits the porosity determination only for macro- and mesopores,[31,32] and for pore size below 6 nm N_2 adsorption porosimetry is useful. We shall delineate here the effect of polymer concentration and the effect of gelling medium particularly by changing the value of n of the diesters on the pore size of the material. The morphology of the materials, the thermal behavior, and the structure of the porous materials are also delineated.

Experimental Section

Samples. Poly(vinylidene fluoride) (PVF_2) is a product of Aldrich Chemical Co. The weight-average molecular weight ($\bar{M}_w$) of the sample is 1.8×10^5, and the polydispersity index is 2.54 as reported by the company. The PVF_2 sample was recrystallized from its 0.2% solution in acetophenone, washed with methanol, and was finally dried in a vacuum at 60 °C for 3 days. The diesters, diethyl adipate (DEA), diethyl suberate (DES), and diethyl azelate (DEAZ) were purchased from Lancaster Synthesis, Morecambe, England, and were used as received.

Gel Preparation. The PVF_2 diester gels were prepared by taking a weighed amount of polymer and solvent in glass tubes (8 mm in diameter), and they were degassed by the repeated freeze–thaw technique. They were then sealed in a vacuum (10^{-3} mmHg) and were made homogeneous at 180 °C for 2 h with occasional shaking. The tubes were then quenched to room temperature (30 °C) to produce the gel.

Preparation of Porous Material. The PVF_2–diester gels were taken out from the sealed tubes by breaking the seals and were kept immersed in cyclohexane in a Petri dish at room temperature (30 °C). Cyclohexane was replaced by fresh batches to drive the replacement equilibrium faster in every 12 h. Such a process was repeated for 6–7 days and was preliminarily tested for complete replacement of ester by pouring the supernatant liquid on a white paper. The absence of an oily spot on the paper primarily indicates the absence of diester in the PVF_2 matrix. Then the cyclohexane was decanted, and the gel was dipped into methanol for 1 day with two times change by fresh methanol. They were then dried in a vacuum at 60 °C for 3 days. The removal of solvent is finally tested from FTIR spectroscopy of the dried gels (Supporting Information Figure 1). The methanol leaching was found necessary as without it a small ⟩C═O peak at 1736 cm^{-1} was observed. However methanol leaching followed by drying do not exhibit any FT-IR peak corresponding to ⟩C═O vibration. Again, only methanol treatment of the gel produces a white precipitate, as it is a strong nonsolvent of PVF_2.

Characterization of the Porous Material. The morphology of dried gels was recorded in a field emission scanning electron microscope (FE-SEM) apparatus (JEOL, JSM-6700F). The samples were used directly without any metal coating and observed at 1 kV. The FT-IR studies were done on dried samples in a Nicolet Instrument [Magna IR-750 spectrometer (series 11)]. The dried gels were mixed with KBr to make pellets and were scanned to an average over 40 s. The WAXS studies of the dried gels were performed by a Seifert X-ray

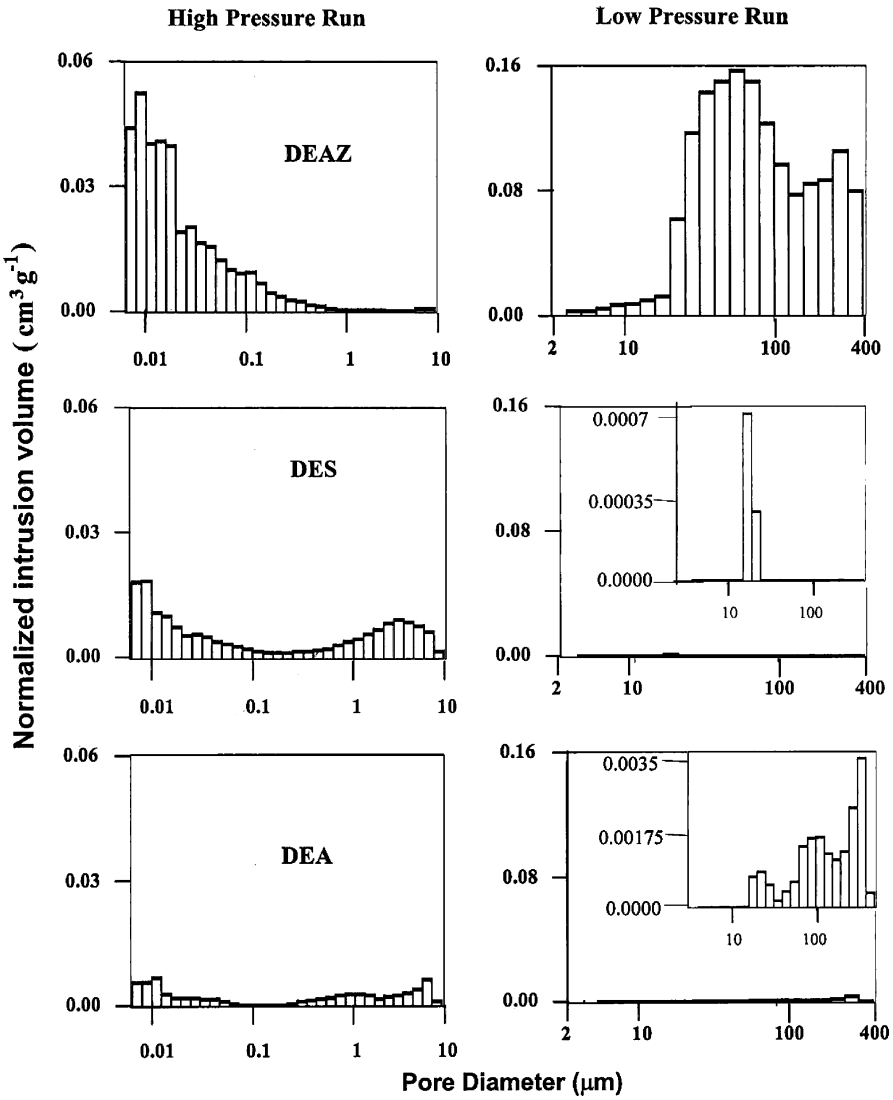

Figure 1. MIP histograms (both high pressure and low pressure) of PVF_2 samples obtained after drying PVF_2–DEAZ, PVF_2–DES, and PVF_2–DEA gels (polymer concentration 10% w/v).

diffractometer (C-3000) using nickel-filtered Cu Kα radiation with a parallel beam optics attachment. The instrument was operated at a 35 kV voltage and a 30 mA current and was calibrated with a standard silicon sample. The samples were scanned from $2\theta = 2°$ at the step scan mode (step size 0.03°, preset time 2 s), and the diffraction pattern was recorded using a scintillation counter detector. For thermal investigation a Perkin-Elmer differential scanning calorimeter (DSC-7) working under a nitrogen atmosphere was used in the work. The instrument was calibrated with indium for each set of experiments. About 3 mg of the samples was taken in aluminum capsules and heated from 50 to 227 °C at a heating rate of 40 °C/min. The higher heating rate was chosen to avoid melt recrystallization.[33,34]

Porosity Measurement. For porosity measurement both mercury intrusion porosimetry (MIP) and N_2 adsorption porosimetry were used. The former was used to measure pore diameter >6 nm, and for pores between 3 and 6 nm the N_2 adsorption method was used. The mercury intrusion porosimetry was done using the instrument Poremaster 33 (Quantachrome Instrument). Two pressure ranges were applied; e.g., low-pressure range (0.5–50 psi) was used to measure pores >10 μm, and high-pressure range (20–34000 psi) was used to measure pore size <10 μm. Blank correction was made using α-Al_2O_3 beads. The sample was introduced in a penetrometer having a stem volume 0.5 cm^3 (Quantachrome) and was at first kept in a low-pressure chamber, and both intrusion and extrusion runs were recorded. After completion of the experiment the penetrometer was transferred to the high-pressure chamber, and the pressure was applied by hydraulic means. Both intrusion and extrusion runs were made as earlier. The data were analyzed by Porowin-32 software. The N_2 adsorption porosimetry was used to measure pores <6 nm, and for this purpose the SA 3100 surface area and pore size analyzer Instrument (Beckman Coulter) was used. The BJH method was used to measure the pore diameter, using SA view software. The desorption data were used to measure BJH pore diameter and pore volume.

Results and Discussion

1. Effect of Intermittent Chain Length of Diesters. In Figure 1 MIP histograms of PVF_2 dried from different gelling media, e.g. diethyl adipate (DEA), diethyl suberate (DES), and diethyl azelate (DEAZ), are presented. Both high-pressure and low-pressure histograms of each sample are shown in the figure. A comparison of histograms is made in the same scale for the high-pressure histogram of each sample, and the same is true for the low-pressure histogram. However, the scales for high- and low-pressure histograms are different. It is apparent from the figure that the DEAZ-dried PVF_2 sample has a significant amount of both meso- and macroporosity. But both the porosity gradually decreases with decreasing number of intermittent

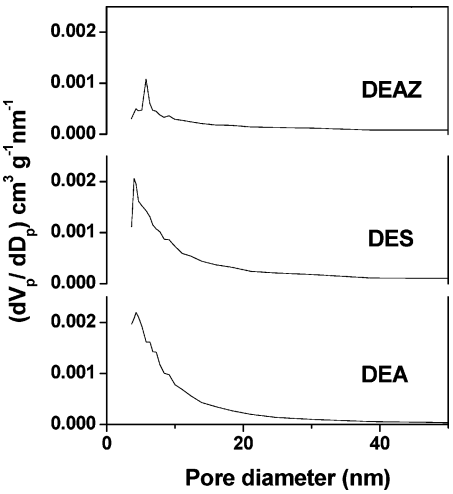

Figure 2. Pore volume distribution curve (desorption, BJH method) obtained from nitrogen adsorption porosimetry of the indicated samples of Figure 1.

carbon atoms "*n*" in the diesters. This may be explained from the fact that the PVF_2 fibrils derived from diester with larger "*n*" are finer than those disters of smaller "*n*" as reported earlier.[23] As a result, there are large cages of solvent molecules among the fibrils causing larger concentration of macropores. Also, the PVF_2–DEAZ complex is the most stable than those of the complexes with the diesters of lower *n*,[23] causing an effective replacement by guest molecule which on drying retains the calthrate structure. On the other hand, weaker polymer–solvent complexes are liable to the collapse of PVF_2 strands to form thicker fibrils during drying, and consequently nanopore concentration is lower. It is noteworthy that the minimum pore diameter in the DEAZ-dried PVF_2 system is 6 nm measured from the MIP method. However, we expect lower pore diameter from the model (Scheme 1), but it is the minimum pore diameter that can be measured from the MIP method. In the following section N_2 adsorption porosimetry will be discussed to show that there are pores lower than 6 nm in the above materials. The highest pore size found for this system from MIP hystograms is 400 μm.

In Figure 2, the pore size distribution curves obtained from nitrogen adsorption porosimetry are presented for the same samples. It is apparent from the figure that minimum size of pores measured is 3.6 nm, and it is the limitation of the instrument. Furthermore, there is a maximum in the distribution curves, e.g., at 6, 4.01, and 4.3 nm for PVF_2 samples dried from DEAZ gel, DES gel, and DEA gel, respectively. It signifies that the maximum number of nanopores have diameter = 6, 4.01, and 4.3 nm for PVF_2–DEAZ, PVF_2–DES, and PVF_2–DEA systems, respectively. It is noteworthy that due to limitation of the instrument we could not measure any pore of diameter 1 nm, which has been depicted from the molecular model (Scheme 1). Anyway, these results signify that a thickness of 3–5 solvent molecules remain intercalated between the PVF_2 chains in the gel. But the possibility of single solvent molecule intercalation cannot be ruled out.

Now we would like to compare the pore volume and surface area of the samples. In Table 1 the pore volume obtained from MIP (>6 nm) and N_2 adsorption porosimetry (<6 nm pore size) are presented. It is apparent from the table that pore volume values have the order DEAZ > DES > DEA from the samples with 10% (w/v) PVF_2 concentration in the gel. This is due to finer structure of the fibrils and greater stability of the polymer solvent complexes with increasing "*n*" of the diesters.[23] Also, the total surface areas of the samples follow the same order; e.g., it decreases with decreasing "*n*". The surface area obtained from high-pressure method is much higher than that of low-pressure method, indicating nanopores have larger surface area than the macropores.

In Figure 3a the hysteresis loops of MIP histograms (high pressure) for intrusion and extrusion processes are presented. It is apparent from the figure that there is hysteresis in all the three samples. This signifies that there are some "interconnected" or "ink bottle" type pores which retain some mercury during extrusion. It is apparent that the PVF_2 sample dried from DEAZ gel shows greater interconnectivity than that of the others. In Figure 3b the hysteresis loops of nitrogen adsorption porosimetry are presented. Here also the hysteresis loops are clearly seen, and the loops are not complete, probably due to the very low rate of N_2 desorption. However, both the hysteresis loops indicate some interconnectivity between the pores of nanodimensions. This interconnectivity between the pores may be supported from the three-dimensional percolation model obeyed by these gels.[22,27,28,35,36]

The X-ray diffractograms (Figure 4) of the samples clearly present the presence of α-polymorphic PVF_2 in the porous material.[37–39] So the drying processes involving the replacement by a guest molecule (cyclohexane) and subsequent leaching by methanol do not change the polymorphic structure of PVF_2 as the solvent subtracted FT-IR spectra of these gels also indicate α-polymorphic structure.[23] From a comparison of the diffractograms at lower angles it is clear that there are some small peaks for the PVF_2–DEAZ system at 2θ = 2.4, 3.45, 4.15, and 5.45° corresponding to d_{hkl} values of 37, 25.5, 21.3, and 16.2 Å, respectively. This may arise from the meso- and micropores of different dimensions.[40] In the other samples no such peaks are observed corresponding to the above d_{hkl} values. It might be due to the reason that the PVF_2–DEAZ complex is the most stable, and all the pores are retained during the drying process. As the interstrand distance between the two PVF_2 chains

Table 1. Pore Volume and Surface Area of PVF_2 Samples Prepared from Gels in Different Diesters and Also at Different Concentrations of PVF_2 Obtained from MIP and Nitrogen Adsorption Porosimetry

		pore volume (cm^3/g)					surface area (m^2/g)				
		MIP method (>6 nm)			BJH	total pore	MIP method (>6 nm)			BJH	total surf.
solvent	concn of polymer (% w/v)	low	high	total	(<6 nm)	vol (cm^3/g)	low	high	total	(<6 nm)	area (m^2/g)
DEAZ	10	1.47	0.34	1.81	0.002	1.812	0.11	95.0	95.11	1.27	96.38
	25	0.003	1.24	1.243	0.002	1.245	0	23.65	23.65	1.51	25.16
	50	0	0.17	0.17	0.002	0.172	0	12.3	12.3	1.2	13.5
DES	10	0.001	0.17	0.171	0.004	0.175	3.57	30.22	33.79	3.57	37.36
DEA	10	0.02	0.07	0.09	0.006	0.096	0.01	10.56	10.58	4.42	15.0

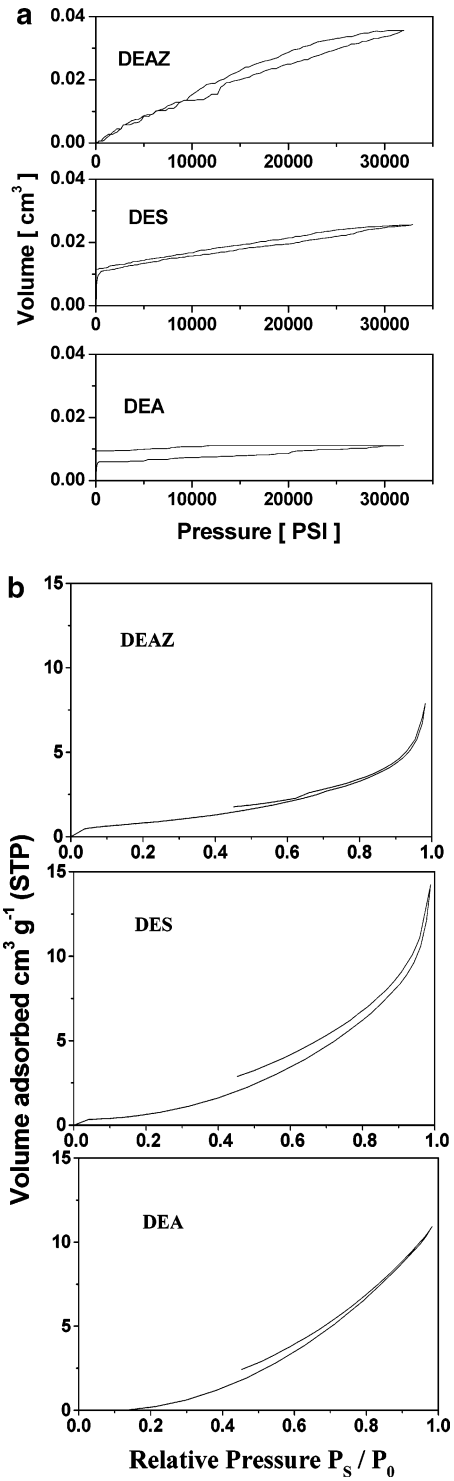

Figure 3. (a) Hysteresis loop of intrusion (lower curve) and extrusion (upper curve) obtained from high-pressure MIP histograms of the indicated samples of Figure 1. (b) N_2 adsorption (lower) and desorption (upper) isotherm of PVF_2 samples obtained after drying PVF_2−DEAZ, PVF_2−DES, and PVF_2−DEA gels (polymer concentration 10%).

for the intercalation of single molecule of DEAZ is 11 Å (Scheme 1) so the above d_{hkl} values approximately correspond to 3, 2, and 1 DEAZ molecules present between the two PVF_2 strands. A definite proof of the above assertion may be achieved from a more sophisticated N_2 adsorption porosimetry using the nonlinear density functional theory (NLDFT) method and is beyond the scope of the present publication.

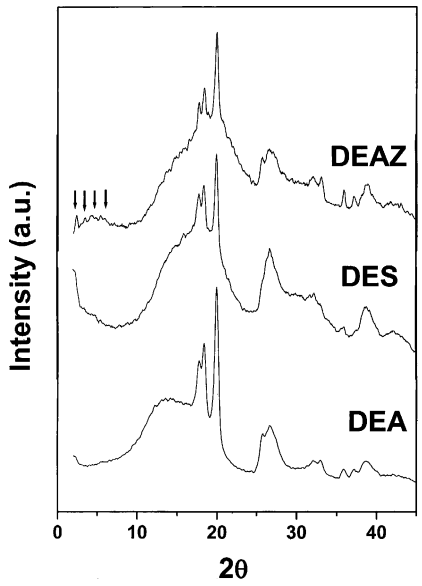

Figure 4. WAXS difractogram of the dried PVF_2 samples obtained from gels in indicated solvents.

In Figure 5 the FE-SEM pictures of all the above samples are presented. All these micrographs indicate presence of fibrillar network containing the porous structure. A comparison of the SEM pictures indicates that the PVF_2/DEAZ system has thinner fibrils than those of the other two systems. The PVF_2 fibrils have average dimensions 40, 68, and 100 nm for samples dried from 10% (w/v) gels in DEAZ, DES, and DEA, respectively. This supports our earlier findings that PVF_2 fibrils become thinner with increasing "*n*" of diesters.[23] Also, pores of different nanodimensions ranging from 37 to 225 nm are clearly seen in the micrographs. A comparison of the pore sizes indicates that the micrograph A has larger number of smaller size nanopores than those of micrographs B and C. Both thicker fibrils and charging of the samples preclude us to get higher magnification pictures in the dried DES and DEA gels. Nonetheless, the presence of multiporosity in these samples can be directly concluded from these micrographs supporting the porosimetric data.

Figure 6a compares the DSC thermograms of the above samples, and all the samples exhibit two melting peaks even at this higher heating rate (40 °C/min) where melt recrystallization is usually absent.[22,23,33,34] A possibility that lower melting peak may arise from residual solvent in polymer−solvent complexes is also completely ruled out as in FTIR spectra of dried samples (Supporting Information Figure 1) no peak characteristic of carbonyl group of diester is present. We, therefore, argue that the two peaks are arising from the melting of porous part and the bulk part of the material separately. The porous part has higher surface energy (due to large surface area), and consequently it melts at lower temperature than the bulk sample.[41] This is clear from part b of the figure where the DSC thermogram of the melt quenched samples under identical condition produce a single peak with a peak temperature of ∼165 °C, corresponding to the bulk melting. The second peak of the samples (Figure 6a) approximately corresponds to the melting of bulk PVF_2, and it increases with decreasing "*n*" of the diester. This is probably due to the fact that the samples with diesters of lower "*n*" collapses more easily during drying forming thicker fibrils which melts at higher temperature. The

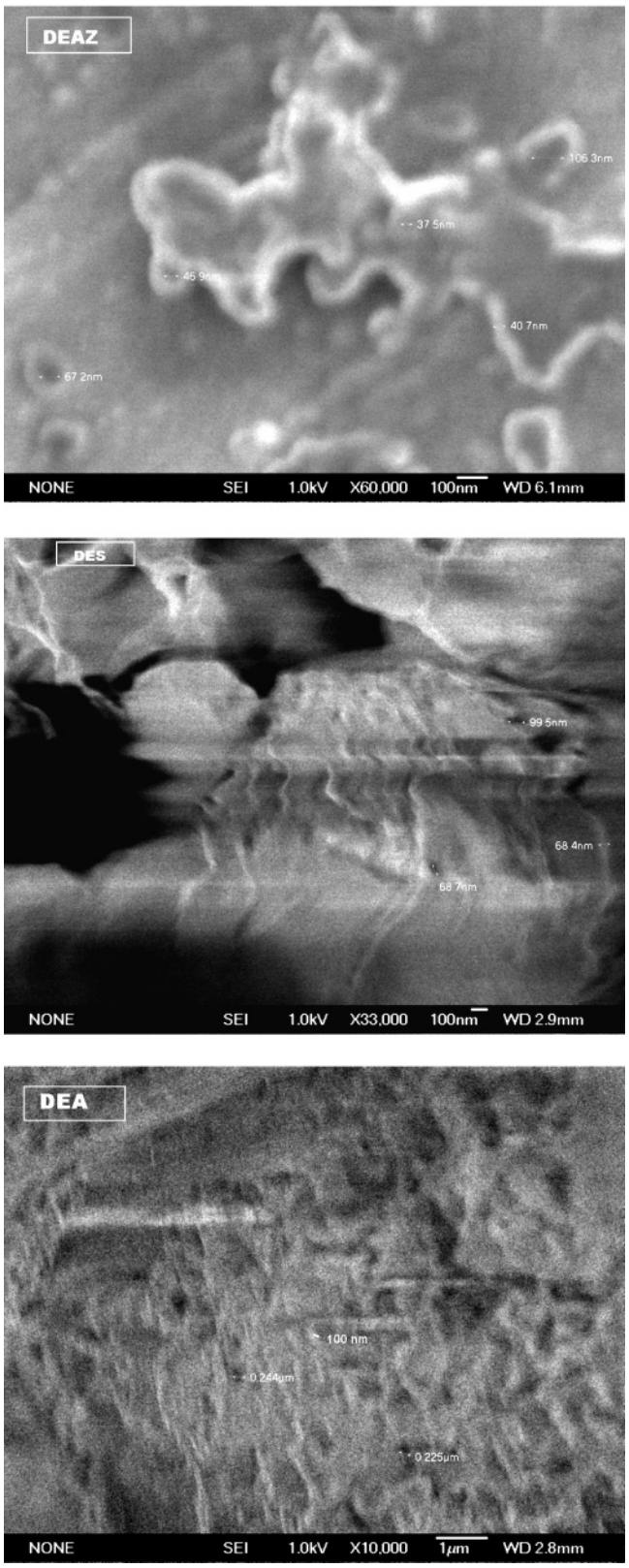

Figure 5. SEM pictures of porous PVF_2 samples obtained after drying PVF_2–DEAZ, PVF_2–DES, and PVF_2–DEA gels (polymer concentration 10%).

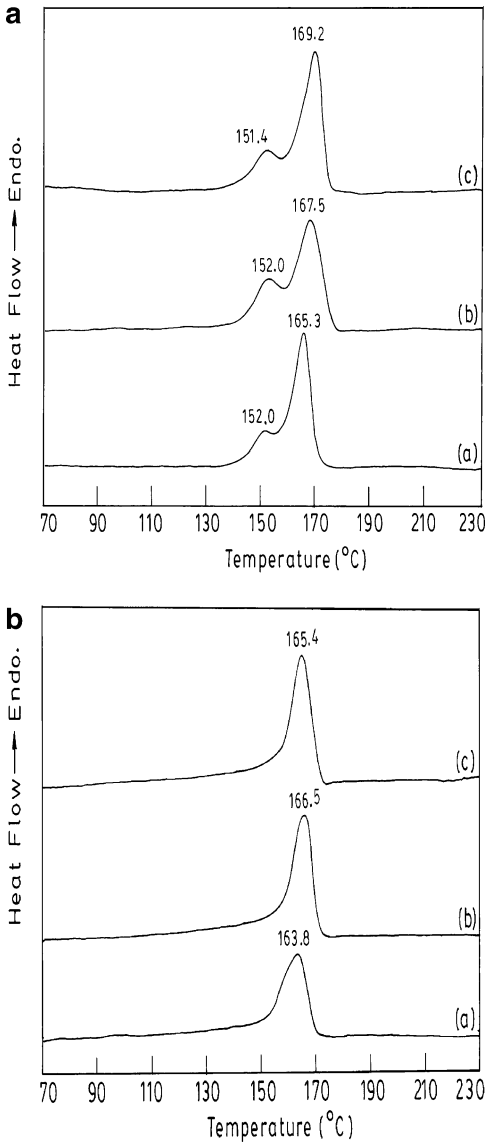

Figure 6. (a) DSC thermograms of porous PVF_2 samples at the heating rate of 40 °C/min for samples dried from 10% (w/v) PVF_2 gels in (a) DEAZ, (b) DES, and (c) DEA. (b) DSC thermograms of the above PVF_2 samples after quenching the melts at 230–50 °C and annealing at 50 °C for 15 min (heating rate = 40 °C/min).

enthalpy of fusion values are found to increase with decreasing "*n*"; e.g., samples dried from PVF_2–DEAZ, PVF_2–DES, and PVF_2–DEA have enthalpy values 60, 70, and 71 J/g, respectively. These enthalpy values probably support that the fibrils are thicker with decreasing "*n*" of the diesters. Again, it may be noted that the peak temperature of higher melting peak of each dried sample is somewhat higher (1–4°) than the melting peak of melt-quenched samples. The more ordered state of the PVF_2 chains in the gel state[22] and in the dried state than that in the melt-quenched state might be the possible reason for the above behavior. This is because during drying of the gel no conformational change of PVF_2 occurred, and melt-quenched crystals are usually somewhat disordered (enthalpy of fusion 48–52 J/g).

2. Effect of Polymer Concentration on Porosity. In Figure 7 the MIP histogram (both high pressure and low pressure) of PVF_2–DEAZ gels dried from different concentration of PVF_2 are compared. The samples dried from lower polymer concentration gel showed larger amount of both meso- and macropores while increasing concentration decreases both meso- and macropores. It is noteworthy that the distribution of pores becomes sharper with increasing PVF_2 concentration. The pore size distribution curves of the above samples obtained

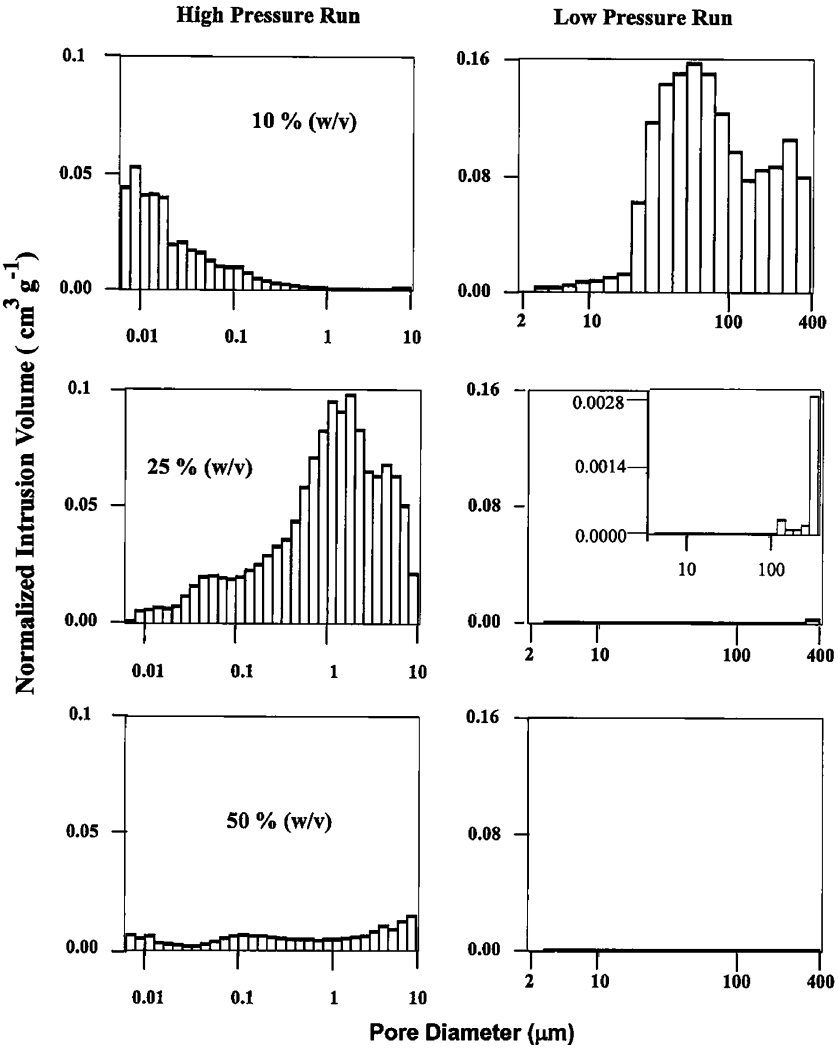

Figure 7. MIP histograms (both high pressure and low pressure) of PVF_2 samples obtained after drying its gels in diethyl azelate at indicated polymer concentrations.

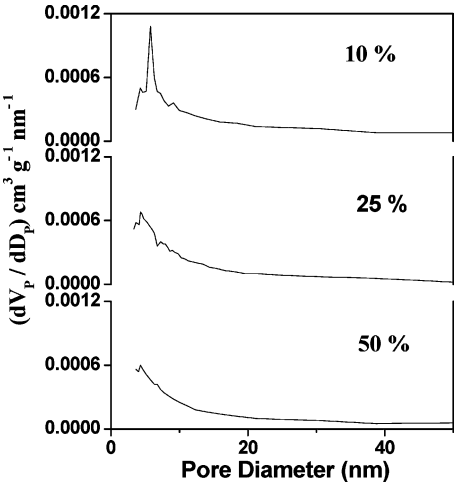

Figure 8. Pore volume distribution curves (desorption, BJH method) obtained from N_2 adsorption porosimetry of the PVF_2 samples obtained after drying its gels in diethyl azelate at indicated polymer concentrations.

by N_2 porosimetry using the BJH technique are shown in Figure 8. The sample dried from 10% (w/v) gel have maximum at 6 nm pore diameter in the 10% PVF_2–DEAZ system, and the maximum occurs at 4.0 and 4.3 nm pore diameter for the 25% and 50% PVF_2–DEAZ system, respectively. It is clear from the figure that with increase in concentration the mesopore concentration in the sample decreases as the height of the distribution peaks decreases with increasing polymer concentration. The hysteresis loop of PVF_2 samples obtained from MIP method with differing PVF_2 concentration (Figure 9) indicates that there is hysteresis in all the samples. The sample dried from the 10% PVF_2–DEAZ gel has prominent hysteresis loop at the high-pressure region whereas samples dried from 25% and 50% DEAZ have prominent hysteresis loop at the low-pressure region. Figure 9 clearly illustrates that the former sample has connectivity among the nanopores while the other samples shows connectivity among larger pore size region. The hysteresis loops of the PVF_2 samples obtained from the N_2 adsorption porosimetry (Supporting Information Figure 2) illustrates that the sample dried from lower polymer concentration of the gel has somewhat larger hysteresis. As a large number of nanopores are produced in these samples, so the interconnectivity between them is large.

If one compares the X-ray diffractograms (Supporting Information Figure 3) of the above samples, the α-polymorphic structure of PVF_2 remains unchanged with polymer concentrations.[37–39] But a careful comparison indicates small peaks at d = 37, 25, 21, and 16 Å for samples dried from lower polymer content samples (cf. Figure 4). Such peaks gradually decrease with increas-

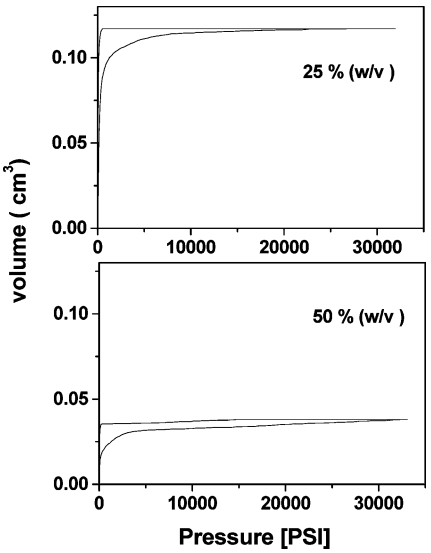

Figure 9. Hysteresis loop of mercury intrusion (lower curve) and extrusion (upper curve) obtained from high-pressure MIP histogram of the PVF_2 samples obtained after drying its gels of different (indicated) polymer concentrations.

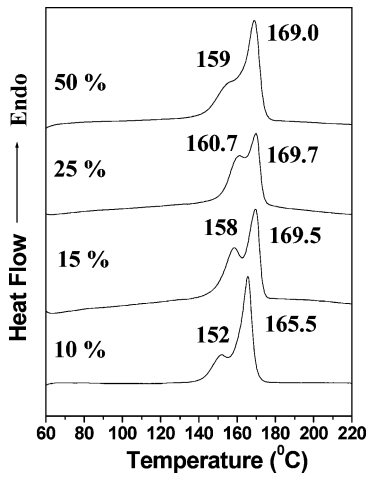

Figure 10. DSC melting endotherms of the dried PVF_2–DEAZ gels from indicated polymer concentration (% w/v) of the gel (heating rate 40 °C/min).

ing concentration supporting the formation of more nanopores in these lower PVF_2 content samples. In Table 1 the pore volume and surface area of the samples are compared. With increasing polymer concentration total pore volume and total surface area decrease abruptly, indicating samples obtained from dilute gels are more porous than those from concentrated gels.

The thermal property of these samples is shown in Figure 10, and there are two melting peaks. As discussed earlier, the lower melting peak corresponds to the melting of crystals at porous portion of the sample and the higher melting peak corresponds to that of the bulk sample. Both the melting peaks increase with increasing polymer concnetration and so also the enthalpy of fusion values. The lower melting peak arises due to higher surface energy of the crystals on the porous sample as discussed earlier. With increasing polymer concentration porous surface area decreases (Table 1), and as a result melting point increases due to lesser surface energy of the crystals. The higher melting peak increases with increasing polymer concentration because of the formation of thicker crystals with increasing polymer concentration. The enthalpy of fusion values are also found to increase; e.g., it is 60, 74, and 77 J/g for samples dried from 10%, 15%, and 25% (w/v) PVF_2–DEAZ gels supporting the formation of thicker crystal with increasing polymer concentration. However, the 50% sample has somewhat lower melting point (0.7 °C) than that of 25% sample, and the enthalpy of fusion value (72 J/g) is also lower. The reason is not yet clear, and it might be due to the very high polymer concentration where some disorder may become introduced in the gel structure and so also in its dried crystals.

Conclusion

Porosity of different dimensions, e.g., micro, meso, and macro sizes, can be introduced in the poly(vinylidene fluoride) sample by drying of its gel in diesters. PVF_2 dried from gels in diesters with increasing number of intermittent carbon atoms (n) produce materials with both increased nano- and macroporosity and with decreasing "n" the porosity decreases. The materials show hysteresis loop in both MIP and nitrogen adsorption porosimetry, indicating ink bottle type or interconnected pore structure in the material. Both pore volume and surface area increases with increasing "n" of the diesters. FE-SEM pictures also exhibit the presence of mesopores and macropores in the materials. The DSC thermograms at higher heating rate (40 °C/min) show two peaks; the lower melting peak may arise due to crystals at pore surface, and the higher melting peak may arise due to crystals in the bulk material. The higher melting peak increases for samples dried from diesters with increasing "n". The drying of the gels were made by replacing the higher boiling diesters with a guest solvent cyclohexane followed by leaching with methanol. With incresing polymer concentration in the gel both nano- and macroporosity decrease.

Acknowledgment. We gratefully acknowledge IFCPAR Grant No. 2808-2 for financial support of the work. We also acknowledge Prof. P. Bhargava and Prof. P. Pramanik of IIT-Kharagpur for their help in porosity measurement.

Supporting Information Available: FTIR spectra of PVF_2, N_2 adsorption and desorption isotherms of PVF_2 samples, and WAXS diffractogram of PVF_2 samples. This material is available free of charge via the Internet at http://pubs.acs.org.

References and Notes

(1) Rao, C. N. R. *Bull. Mater. Sci.* **1999**, *22*, 141.
(2) Hester, J. F.; Banerjee, P.; Won, Y.-Y.; Akthakul, A.; Acar, M. H.; Mayes, A. M. *Macromolecules* **2002**, *35*, 7652.
(3) Ying, L.; Wang, P.; Kang, E. T.; Neoh, K. G. *Macromolecules* **2002**, *35*, 673.
(4) Chen, Y.; Ying, L.; Yu, W.; Kang, E. T.; Neoh, K. G. *Macromolecules* **2003**, *36*, 9451.
(5) Xu, Y.; Zheng, D. W.; Tsai, Y.; Tu, K. N.; Zhao, B.; Liu, Q.-Z.; Brongo, M.; Ong, C. W.; Choy, C. L.; Sheng, G. T. T.; Tung, C. H. *J. Electron. Mater.* **2001**, *30*, 309.
(6) Li, Y.; Chu, L.-Y.; Zhu, J.-H.; Wang, H.-D.; Xia, S.-L.; Chen, W.-M. *Ind. Eng. Chem. Res.* **2004**, *43*, 2643.
(7) Akthakul, A.; Salinaro, F.; Mayes, A. M. *Macromolecules* **2004**, *37*, 7663.
(8) Saunier, J.; Gorecki, W.; Alloin, F.; Sanchez, J. Y. *J. Phys. Chem. B* **2005**, *109*, 2487.
(9) Pedireddi, V. R.; Chatterjee, S.; Ranganathan, A.; Rao, C. N. R. *J. Am. Chem. Soc.* **1997**, *119*, 10867.
(10) Ranganathan, A.; Pedireddi, V. R.; Rao, C. N. R. *J. Am. Chem. Soc.* **1999**, *121*, 1752.

(11) Van de Witte, P.; Dijkstra, P. J.; Van den Berg, J. W. A; Feijen, J. *J. Membr. Sci.* **1996**, *117*, 1.
(12) Matsuyama, H.; Takida, Y.; Maki, T.; Teramoto, M. *Polymer* **2002**, *43* 5243.
(13) Siripurapu, S.; Coughlan, J. A.; Spontak, P. J.; Khan, S. A. *Macromolecules* **2004**, *37*, 9872.
(14) Krause, B.; Sijbesma, H. J. P.; Munuklu, P.; van der Vegt, N. F. A.; Wessling, M. *Macromolecules* **2001**, *34*, 8792.
(15) Guerra, G.; Manfredi, C.; Musto, P.; Tavone, S. *Macromolecules* **1998**, *31*, 1329.
(16) Reversible polymeric gels and related systems: Russo, P. S., Ed.; *ACS Symp. Ser.* **1986**.
(17) Guenet, J. M. *Thermoreversible Gelation of Polymers and Biopolymers*; Academic Press: London, 1992.
(18) Berghmans, H. In *Integration of Fundamental Polymer Science and Technology*; Larnstra, P. J., Kleintiens, L. A., Eds.; Elsevier Applied Science: London, 1988; Vol. 2, p 296.
(19) Guenet, J. M.; Ray, B.; Elhasri, S.; Marie, P.; Thierry, A. *NATO Sci. Ser. IV: Earth Environ. Sci.* **2003**, *24*, 191.
(20) Lovinger, A. J. In *Developments in Crystalline Polymers 1*; Basset, D. C., Ed.; Elsevier Applied Science: London, 1981; p 195.
(21) Wang, D.; Li, K.; Teo, W. K. *J. Membr. Sci.* **1999**, *163*, 211.
(22) Dikshit, A. K.; Nandi, A. K. *Macromolecules* **1998**, *31*, 8886.
(23) Dikshit, A. K.; Nandi, A. K. *Macromolecules* **2000**, *31*, 2616.
(24) Gajewski, K. E.; Gillberr, M. H. In *Advances in Molecular Modeling*; Liotta, D., Ed.; Jai Press: Greenerick, CT, 1990; Vol. 2.
(25) Zallen, R. *The Physics of Amorphous Solids*; John Wiley and Sons: New York, 1983; p 135.
(26) Stauffer, D.; Coniglio, A.; Adam, M. *Adv. Polym. Sci*. **1982**, *44*, 103.
(27) Mal, S.; Nandi, A. K. *Polymer* **1998**, *39*, 6301.
(28) Chou, C. M.; Hong, P. D. *Macromolecules* **2003**, *36*, 7331.
(29) Guenet, J.-M. *J. Rheol.* **2000**, *44*, 947.
(30) Daniel, C.; Alfano, D.; Guerra, G.; Musto, P. *Macromolecules* **2003**, *36*, 1713.
(31) Leon, C. A.; Leon, Y. *Adv. Colloid Interface Sci.* **1998**, *76*−*77*, 341.
(32) Abell, A. B.; Willis, K. L.; Lange, D. A. *J. Colloid Interface Sci.* **1999**, *211*, 39.
(33) Prest, W. M., Jr.; Luca, D. J. *J. Appl. Phys.* **1975**, *46*, 4136.
(34) Nandi, A. K.; Mandelkern, L. *J. Polym. Sci., Polym. Phys. Ed.* **1991**, *29*, 1287.
(35) Mal, S.; Maiti, P.; Nandi, A. K. *Macromolecules* **1995**, *28*, 2371.
(36) Dikshit, A. K.; Nandi, A. K. *Langmuir* **2001**, *17*, 3607.
(37) Lando, J. B.; Doll, W. W. *J. Macromol. Sci., Phys.* **1968**, *2*, 205.
(38) Hasegawa, R.; Takahashi, Y.; Chatani, Y. *Polym. J.* **1972**, *3*, 600.
(39) Bechmann, M. A.; Lando, J. B. *Macromolecules* **1981**, *14*, 40.
(40) Zhang, H.; Sun, J.; Ma, D.; Bao, X.; Klein-Hoffmann, A.; Weinberg, G.; Su, D.; Schlogl, R. *J. Am. Chem. Soc*. **2004**, *126*, 7440.
(41) Mandelkern, L. In *Comprehensive Polymer Science*; Allen, G., Ed.; Pargamon Press: Oxford, 1989; Vol. 2, p 363.

MA050601G